Optimization and Microfabrication of High Performance Silicon-Based MEMS Microspeaker

Iman Shahosseini, Elie Lefeuvre, Johan Moulin, Emile Martincic, Marion Woytasik, and Guy Lemarquand, *Senior Member, IEEE*

***Abstract*— A novel structure of electrodynamics microelectromechanical systems (MEMS) microspeaker designed for mobile electronics is proposed in this paper. The originality of the device lies on the use of a rigid silicon membrane suspended by highly flexible silicon springs, contrary to most MEMS and non-MEMS microspeakers, which use polymer diaphragms. Important rigidity of the membrane and high linearity of the magnetic actuation conferred outstanding sound quality. The design of the silicon springs enabled large out-of-plane displacement of the membrane, which improved the bass rendering and the acoustic intensity over the whole bandwidth. The low density of silicon material helped to reduce the mobile mass and thus improved the microspeaker efficiency. A prototype with a membrane diameter of 15 mm and a thickness of 20 μm is microfabricated and characterized. The silicon springs enabled out-of-plane displacement of more than 300 μm. Acoustic intensity of 80-dB SPL is measured at 10 cm with 500-mW input power. This sound pressure level is obtained at frequencies from 330 Hz up to 70 kHz. Thanks to the membrane backside microstructure, most of the membrane proper modes are shifted out of the audible bandwidth. The measured electroacoustic efficiency is almost three times better than that of conventional microspeakers.**

***Index Terms*— Electromagnetic, microelectromechanical systems (MEMS), microspeaker, planar coil, silicon membrane.**

I. Introduction

TODAY, mobile electronic devices know a flourishing market of highly demanding users who tend towards products with more integrated functions, smaller physical size, higher autonomy, and better performance. This tendency also concerns the acoustic performance of multimedia mobile systems. Indeed, cellular phones, notebooks, tablets, still cameras and camcorders have to reproduce speech and music signals with improved loudness and sharpness. At the same time, each function should have reduced power consumption. Thus, the global power consumption tends to be reduced, so extending the device playback time.

Concerning the power consumption of audio systems, it is mainly determined by the microspeaker efficiency. Indeed, amplifiers used in sound reproduction systems have pretty good efficiency, typically between 70% and 90% [1], whereas microspeakers have very poor electroacoustic efficiency, typically lower than 0.001% [2]–[4]. This last point explains why the power consumption of audio systems remains high compared to other functions. For instance, in the case of cellular phones the audio system consumes almost a quarter of the overall device power [5].

Concerning the sound quality, the amplifiers performances are also much better than those of the microspeakers. Class-D amplifiers, which are commonly used in mobile devices, provide audio signals with low harmonic distortion (THD), low intermodulation distortion (IMD), and high signal-noise-ratio (SNR), in accordance with Hi-Fi standards [6], [7]. The poor sound quality, which is a typical characteristic of the majority of the mobile devices, is actually due to the microspeakers imperfections [5].

These conventional microspeakers are actually miniaturized structures of classical loudspeakers. Unfortunately, size reduction has a negative impact on the electroacoustic performances. For the sake of integration, the radiator surface, its mechanical suspensions, and the electromagnetic part are simplified. This results in narrow bandwidth response with nonlinearities, which deteriorate the sound quality [2]–[4].

With classical technology, the performances of microspeakers have reached some limits. This is partly due to the used materials. For instance, membranes of conventional microspeakers are made of plastic or polymers, which are too soft to provide a good radiator surface. Moreover, with this type of technology it is difficult to get high dimensional precision which could help to improve the performances. At this point, manufacturing precision and reproducibility of microsystems technologies offer promising opportunities to go beyond the limits of classical manufacturing technologies. Low cost production due to batch processing could be another advantage for industries to answer a market of more than one billion microspeakers per year [8]. MEMS technology also gives the possibility to integrate transducers and amplifiers into the same package, so-called "system in package", and thus reduce the audio system overall size [9], [10].

Based on MEMS technology, the present study aims at both reducing the energy consumption of microspeakers, with an

Manuscript received February 13, 2012; revised April 5, 2012; accepted July 27, 2012. Date of publication August 23, 2012; date of current version January 7, 2013. This work was supported by French National Research Agency. The associate editor coordinating the review of this paper and approving it for publication was Dr. Patrick Ruther.

I. Shahosseini, E. Lefeuvre, J. Moulin, E. Martincic, and M. Woytasik are with Institut d'Electronique Fondamentale, University of Paris-Sud, Orsay 91405, France (e-mail: iman.shahosseini@u-psud.fr; elie.lefeuvre@u-psud.fr; johan.moulin@u-psud.fr; Emile.Martincic@u-psud.fr; marion.woytasik@u-psud.fr).

G. Lemarquand is with the Laboratoire d'Acoustique de l'Université du Maine, Avenue Olivier Messiaen, Le Mans 72085, France (e-mail: guy.lemarquand@univ-lemans.fr).

Color versions of one or more of the figures in this paper are available online at http://ieeexplore.ieee.org.

Digital Object Identifier 10.1109/JSEN.2012.2213807

efficiency goal of 0.01%, and ameliorating the sound quality. A sound pressure level (SPL) of 80 dB at 10 cm within 300 Hz to 20 kHz range is the target of this work.

Former works in field of MEMS microspeakers have mainly focused on hearing aid or headphone applications. Reported devices had a radiator surface smaller than 25 mm^2 [11]–[23]. Owing to its larger radiator surface, the MEMS microspeaker presented in this work has much higher SPL capability. Its sound intensity is high enough for applications such as free-hand mode of mobile phones. As it will be detailed in the following sections, its dimensions are closer to those of classical microspeakers than those of the aforementioned MEMS microspeakers.

Several actuation principles have been investigated for microspeakers. Among them, three major types can be highlighted: electrostatic, piezoelectric, and electrodynamic (Table I). Besides, the use of electrostrictive effect in polymer films and thermo-acoustic properties of carbon nanotubes must also be mentioned [24], [25]. The electrodynamic actuation is used in most of classical microspeakers, but the full integration of magnetic materials remains difficult in MEMS today's technology. In spite of their simple fabrication, electrostatic actuators are limited both in displacement and in force magnitude, and they also require high driving voltage. Piezoelectric actuation enables wider displacement and stronger force density, but non-linear behavior and hysteresis of piezoelectric materials are major drawbacks for audio applications. In addition, integrated piezoelectric thick films are sensitive to residual stress, which reduces the devices reproducibility [9], [26]. Concerning thermal actuators, they suffer from large power consumption, so low efficiency [25].

Regarding the objectives of this work, the electrodynamic actuation is actually the most interesting type. Indeed, it enables high power densities and large mechanical displacements. Moreover, its quasi-linear behavior makes possible high fidelity sound reproduction [26].

This paper is organized as follows. First, the architecture of the MEMS microspeaker is presented and compared to previous works. Then, both the membrane and the microcoil dimensions are optimized in section III. Section IV details the microfabrication steps of the device. Finally, electromechanical and electroacoustic characterizations of the device are presented in section V, before the conclusions and perspectives.

II. Microspeaker Structure

Most of former works on MEMS microspeakers presented architectures based on deformable diaphragms. For instance they used polyimide or parylene diaphragms, clamped to the substrate all along their perimeter [11]–[13]. In this way, the diaphragm plays the role of both the radiator surface and the deformable suspension. The so-called drum mode is the fundamental working mode for this kind of structure, with a displacement peak located at the center of the diaphragm. However, from the acoustic point of view, the sound waves should be ideally generated by the displacement of a perfectly flat and rigid surface, so-called piston mode. Indeed, all dynamic deformations of the emissive surface induce sound distortion [27]. Flexible diaphragms have actually many vibration modes which deteriorate the sound quality of the microspeaker. Therefore, the use of a deformable diaphragm is not compatible with high-fidelity performances. Another advantage of the piston mode is the bigger volume of the displaced air comparing to the drum mode when considering the same membrane surface and displacement. Consequently, higher power densities can be obtained with the same radiator surface.

The structure of our MEMS microspeaker is depicted in Fig. 1. The inset shows a part of the membrane microstructure, which contributes to the membrane rigidity. This point makes possible to overcome the membrane deformation obstacle, thus providing a perfect radiator. The very flexible springs were designed to enable large out-of-plane displacement [28]. A planar microcoil was located on top of the membrane. Two ring-shape permanent magnets were attached on both sides of the device, symmetrically to the coil plane.

The driving force $F_{Lorentz}$, so-called the Lorentz force, lies on the interaction between the magnetic field and the coil electric current. This force acting on a wire of length l which carries an electric current I surrounded by a magnetic flux density B can be written as

$$F_{Lorentz} = I.\int_0^l \vec{B}.d\vec{l}. \tag{1}$$

For a planar coil with concentric turns, (1) can be rewritten as

$$F_{Lorentz} = \sum_{i=1}^{N} I.2\pi.R_i.B_r(R_i) \tag{2}$$

where R_i is the radius of the i^{th} turn and $B_r(R_i)$ the radial component of magnetic flux density in the coil plane, observed by the i^{th} turn. Here, the magnetic field is assumed to have the same symmetry axis as the magnets. Consequently, all the elementary forces cancel out each other except for the elementary forces being parallel to the symmetry axis. Thus, the resulting force $F_{Lorentz}$ is perpendicular to the coil-membrane plane.

In practice, the microcoil is fed using two conductor tracks located on top of the suspension beams, which makes the contact with the coil on its bottom side. These tracks are electrically insulated by a SiO_2 film. Two vias enable the electric contact with the coil inner and outer ends.

III. Design of the Microspeaker Parts

Defining the device dimensions is a complex problem because it involves simultaneously the mechanical, electrical, magnetic, and acoustic aspects of the problem. For the sake of clarity we detail first the mechanical side in subsection A, and then the electromagnetic side of the optimization problem in subsection B. The efficiency, which links these two parts together, remains first implicit, and then is detailed in subsection B.

TABLE I
COMPARISON OF DIFFERENT MEMS MICROSPEAKERS

Actuation type	Reference	Material for membrane	Membrane surface	Membrane thickness	Maximum membrane displacement	Maximum SPL	Power consumption	Note
Piezoelectric	[14]	SiN + ZnO	25 mm^2	2.7 μm	-	92 dB at 3 kHz at 0.2 cm		Driving voltage: 6 $V_{peak-peak}$
	[15]	SiN + AlN	-	$\sim$ 3 μm	-	100 dB at 9.3 kHz at 1 cm		Driving voltage: 12 $V_{peak-peak}$
	[11]	SiN + ZnO	9 mm^2	3 μm	1 μm	83.1 dB at 13.3 kHz at 1 cm		Driving voltage: 30 $V_{peak-peak}$
	[16]	SiN + ZnO	4 mm^2	4.7 μm	-	70 dB at 5 kHz at 0.5 cm		Driving voltage: 16 $V_{peak-peak}$
Electrostatic	[17]	Silicon	3.14 mm^2	14 μm	-	112 dB at 127 kHz at 1 cm		Driving voltage: 50 $V_{peak-peak}$
	[18]	Poly-SiC	0.5 mm^2	1 μm	-	73 dB at 16.6 kHz at 1 cm		Driving voltage: 200 $V_{peak-peak}$
Thermoacoustic	[26]	Carbon Nanotubes	900 mm^2 (One layer)	-	-	85 dB at 10 kHz at 5 cm	3 W	
			900 mm^2 (Four layer)		-	95 dB at 10 kHz at 5 cm	12 W	
Electrodynamics	[12]	Polyimide	9.6 mm^2	5 μm	5 μm	93 dB at 5 kHz in 2 cm^3 coupler	320 mW	Coil: 5 μm thick, 100 μm wide Magnet: Nd-Fe-B, 0.6 T 2.6 $\times$ 2.6 $\times$ 3 mm F = 206 μN for 215 mA
	[13]	Polyimide	7 mm^2	22 μm	0.8 μm	106 dB at 1 kHz in 2 cm^3 coupler	0.13 mW	Coil: 10 μm thick, 100 μm wide, 100 μm inter-space, 10 μm multilayer spacing, 1.5 Ω Soft magnet: 1 mm diameter, 10 to 20 μm thick Permanent magnet: 1 T, 20 mm outer diameter, 4 mm inner diameter, 0.5 mm thickness F = 37 μN for 20 mA
	[19]	PDMS	9.6 mm^2	3.3 μm	8.3 μm	106 dB at 1 kHz in 2 cm^3 coupler	1.76 mW	Coil: 200 μm wide Magnet: B_r = 0.475 T F = 0.205 μN for 65.6 μA
	[20]	NiCoFe	19 mm^2	80 μm	12 μm	106 dB at 1 kHz in 2 cm^3 coupler	0.5 mW	Coil: 240 turn, 125 Ω 2 magnets each Hc = 160 kA/m height = 250 μm F = 10 mN for 10 mA
	[21]	Poliymide	4.9 mm^2	2 μm	17 μm	108 dB in 2 cm^3 coupler	3.4 mW	Coil: 50 μm wide, 15 μm thick, 1.6 mm diameter Magnet: 1.59 mm diameter Nd-Fe-B for 100 mA
	[22]	-	-	-	4.25 μm	70 dB at 5 kHz	-	Coil: 0.12 mm diameter Magnet: 6 mm diameter Nd-Fe-B
	[23]	Poliymide	7 mm^2	7 μm	8 μm	96 dB in 2 cm^3 coupler	-	
	This paper	**Silicon**	**177 mm^2**	**20 μm + 300 μm ribs**	**300 μm**	**80 dBat 0.33 kHz at 10 cm**	**0.5 W**	Coil: 35 μm wide, 30 μm thick, 20 μm inter-space, 10 Ω Magnet: 3 mm thick, 1.5 T, inner diameter 15 mm, outer diameter 21 mm Nd-Fe-B

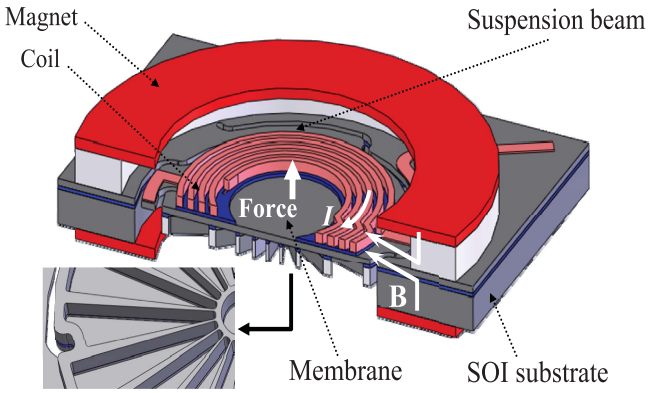

Fig. 1. Cut view of the microspeaker. Inset: backside structured membrane.

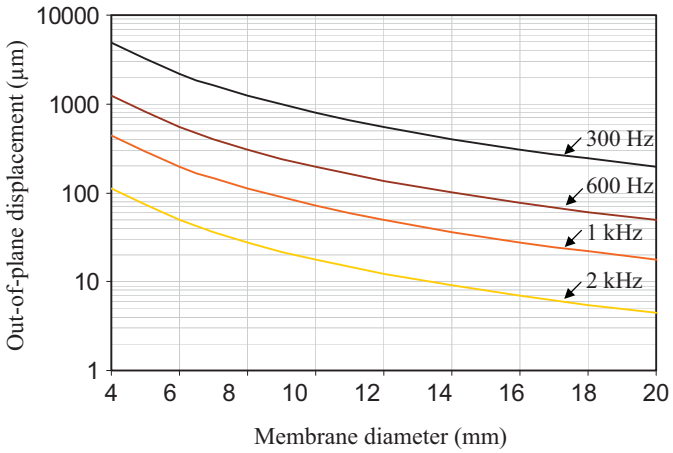

Fig. 2. Membrane out-of-plane displacement as a function of its diameter for 80-dB SPL at 10 cm, for 300, 600, 1000, and 2000 Hz working frequencies.

A. Membrane

The first step to determine the membrane dimensions is to consider the volume of air which should be displaced. The air volume itself depends on the acoustic power that the microspeaker is supposed to produce at a given frequency. All these parameters are linked together by the expression given in (3), where d is the membrane diameter, x_{peak} its out-of-plane peak displacement, f the working frequency, and $P_{acoustic}$ the acoustic power [27], [29]

$$P_{acoustic} = 0.27 d^4 f^4 x_{peak}^2. \tag{3}$$

From (3) it can be deduced that acoustic power is proportional to the displaced air volume squared $(x_{peak}.d^2)^2$. For a spherical acoustic radiation, the acoustic power can be defined as

$$P_{acoustic} = 10^{\frac{L_{dB}}{10}} \times 10^{-12} \times 4\pi \times r^2 \tag{4}$$

with L_{dB} the sound pressure level at distance r from the acoustic source [27].

According to (4), 80 dB SPL at 10 cm corresponds to radiated acoustic power of 12.6 μW. For a given radiated acoustic power, (3) shows that the lower the working frequency is, the higher the displaced air volume is. For instance, to radiate 12.6 μW acoustic power, 60 mm^3 and 1.3 mm^3 air volume should be displaced respectively at 300 Hz and 2 kHz. Thus, generating high SPL at low frequency is challenging in terms of mechanical design of the MEMS. This point is highlighted by the curves drawn on Fig. 2, which show the membrane diameter as a function of the membrane peak displacement for different working frequencies.

Once considering the minimum working frequency of 300 Hz, Fig. 2 shows that for diameters smaller than 9 mm, out-of-plane displacements larger than 1 mm are required. Such displacements are actually difficult to achieve using MEMS technologies. Conversely, with membrane diameters bigger than 18 mm, less than 250 μm out-of-plane displacement is needed. However, in this case the device would become too cumbersome to be integrated in mobile devices. In addition, larger membrane increases the device final cost. A membrane of 15 mm in diameter can be taken as a good trade-off between these limits. The radiator surface remains below 2 cm^2, which looks acceptable regarding the device applications. For this membrane surface, an out-of-plane displacement of 300 μm should be provided by the suspension beams at 300 Hz. From mechanical stress point of view, this is the extreme operating condition for the suspension part, since working in higher frequencies or lower acoustic power asks for smaller displacements.

Two factors have to be taken into account to determine the membrane thickness: the membrane mass and the membrane natural modes. Indeed, as it will be detailed later, the membrane has to be as light as possible to keep up the electroacoustic efficiency. Moreover, as mentioned before concerning the acoustic quality, the membrane should not present natural modes in the frequency range of interest. For instance for a free circular membrane, the modal frequencies are determined by

$$f_i = \frac{2}{\pi}.\left(\frac{\beta_i}{d}\right)^2.\sqrt{\frac{E}{\rho}.\frac{h^2}{12(1-\upsilon^2)}} \tag{5}$$

where β_i is the characteristic constant of the mode i, d the membrane diameter, h its thickness, E the Young's modulus, ρ the material density, and υ the Poisson coefficient [30]. Eq. (5) shows that for a given diameter, the modal frequencies depend on the E/ρ ratio and the thickness h.

It is possible to express the mass M independently from the thickness of the membrane by extracting h from (5) and replacing this parameter into the basic expression of the mass in (6)

$$M = \frac{\rho.h.\pi.d^2}{4} = \frac{\pi^2.d^4.f_1}{8\beta_i}.\sqrt{12.\frac{\rho^3}{E}.(1-\upsilon^2)}. \tag{6}$$

For our application, the lowest modal frequency should ideally be higher than 20 kHz. That is to say that the frequency f_1, corresponding to the first vibration mode, should be set higher than 20 kHz. To do so, according to (6), the E/ρ^3 ratio should be as high as possible in order to minimize the mass M. This ratio was chosen as a figure of merit for choosing the membrane material. It should be noted that this ratio is also found for other geometries such as clamped beams and plates [30]. The Poisson coefficient was not taken into account due to its second-order influence.

TABLE II
FIGURE OF MERIT FOR DIFFERENT MATERIALS

Material [36], [37]	ρ (gr/cm^3)	E (GPa)	E/ρ^3
C (Diamond)	3.52	1000	22.9
Si	2.33	165	13.0
SiO_2	2.2	107	10.0
Mg	1.74	45	8.54
Al_2O_3	3.97	390	6.23
Al	2.7	69	3.50
Ti	4.54	115	1.22
Polyimide	1.43	3.2	1.09
Cr	7.19	298	0.801
Mn, Mo, Ni, Co, Co, Zn, Cu	7.13 – 10.22	96 – 329	0.153 – 0.480

The figure of merit of different materials was calculated and summarized in Table II. As it can be noticed, except for diamond, silicon presents the best properties for the membrane. In addition, this material has the advantage of having a large panel of micromachining processes available.

Eq. (7) quantifies the impact of the membrane mass $M_{membrane}$ on the electroacoustic efficiency η

$$\eta = \frac{\rho.\pi.r^4}{4c}.\frac{1}{R}.\left(\frac{f_{Force}}{M_{coil}+M_{membrane}}\right)^2. \quad (7)$$

Here, ρ is the air density (1.2 kg/m^3 at 20 °C), r the membrane radius (7.5 mm), c the sound speed (343 m/s at 20 °C), R the coil resistance (10 Ω), M_{coil} the coil mass, and f_{Force} the force factor defined as the driving force per current unit [29].

This expression shows that if considering a 10 μm thick membrane and a force factor of 0.35 N/A, the efficiency reaches 0.1%. However, with the help of finite element modeling (FEM), the modal analysis of a free 10 μm thick silicon membrane showed that there exist at least 50 undesirable vibration modes in the considered frequency bandwidth. In particular the drum mode takes place at a very low frequency of 600 Hz. One should notice that this particular vibration mode is known to have an important impact on the transducer sound distortion. Thus, this mode must be shifted to higher frequencies, for which human ear is not sensitive. One solution to do so could be increasing the membrane thickness.

To do so, doubling the thickness would not be enough. Using (5) and setting the first resonance frequency f_1 at 20 kHz and silicon membrane diameter at 15 mm, the thickness should be raised to 320 μm. But the membrane mass would be significantly increased, and thus the efficiency would be dropped down to 5×10^{-6}, which is far behind our objective.

To overcome this problem, we have studied the design of a reinforcing structure for the membrane in order to reduce the membrane mass while shifting the majority of the vibration modes out of the microspeaker bandwidth. Comparison of different designs such as corrugated membrane, hexagonal shape, or crossed beam structure [31]–[33] led us to propose the radial ribbed structures shown in Fig. 3. Previous study

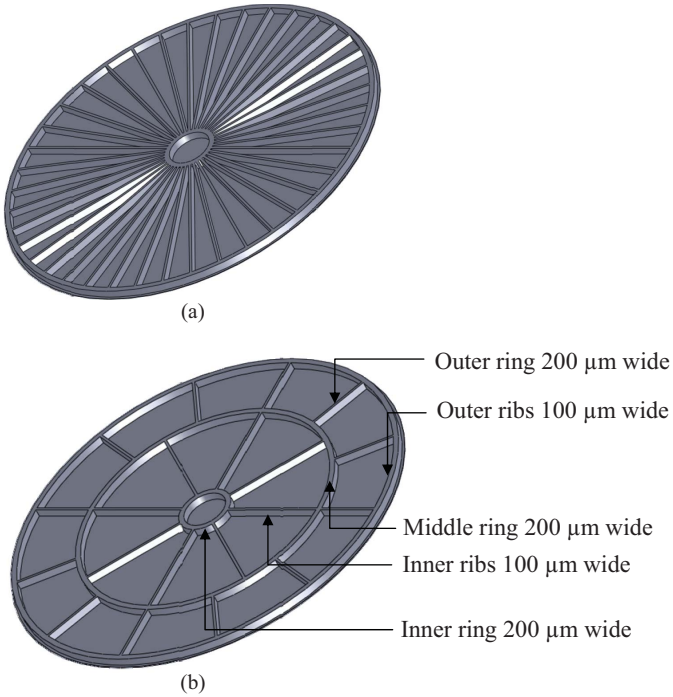

Fig. 3. Microstructured membranes. (a) 40-rib design [34] and (b) ameliorated design.

TABLE III
COMPARISON OF MICROSTRUCTURED AND PLAIN MEMBRANES

Design	Membrane mass (mg)	Coil mass (mg)	Total mass (mg)	Drum mode frequency (kHz)	Modes number	Efficiency
10-μm thick plain membrane	4	2	6	0.62	50	16.15×10^{-4}
20-μm thick plain membrane	8	3	11	1.32	30	6.64×10^{-4}
320-μm thick plain membrane	132	6	138	20.15	1	0.06×10^{-4}
Structured membrane [34]	32	6	53	15.08	3	0.78×10^{-4}
New structured membrane	24	6	31	15.38	2	1.28×10^{-4}

[34] showed that with 40 ribs and one inner and one outer rings (Fig. 3-a), the drum mode is shifted to 15 kHz while the theoretical efficiency meets our objective, as shown in Table III.

For the present structure design, shown in Fig. 3-b, the performances were improved by adding a third middle ring and by modifying the ribs number. Fig. 4 shows that the maximum of the drum mode frequency takes place for a middle ring of 9.7 mm in diameter, with 6 inner and 24 outer ribs. Afterwards,

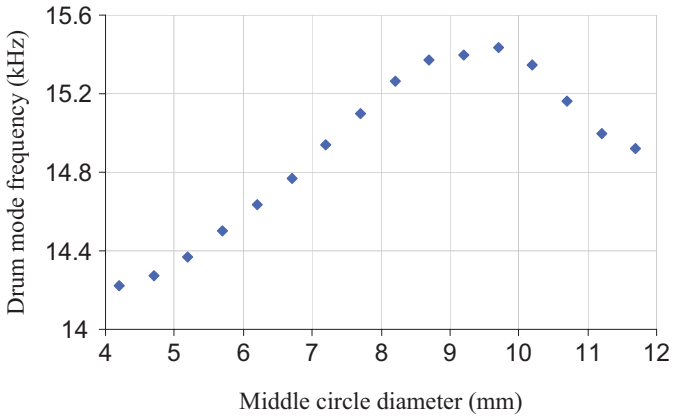

Fig. 4. Drum mode frequency as a function of middle circle diameter for six inner and 24 outer ribs of 100-μm width and 300-μm thickness.

TABLE IV
DRUM MODE FREQUENCY AND MICROSPEAKER EFFICIENCY AS FUNCTION OF DIFFERENT INNER AND OUTER RIBS NUMBER

Outer ribs number	Inner ribs number			
	3	**6**	**8**	**12**
12	13.68 kHz 1.40×10^{-4}	15.10 kHz 1.33×10^{-4}	15.38 kHz 1.28×10^{-4}	15.49 kHz 1.20×10^{-4}
18	13.87 kHz 1.32×10^{-4}	15.33 kHz 1.25×10^{-4}	15.61 kHz 1.21×10^{-4}	15.70 kHz 1.12×10^{-4}
24	13.92 kHz 1.23×10^{-4}	15.43 kHz 1.18×10^{-4}	15.66 kHz 1.13×10^{-4}	15.76 kHz 1.06×10^{-4}
30	13.92 kHz 1.16×10^{-4}	15.42 kHz 1.10×10^{-4}	15.66 kHz 1.07×10^{-4}	15.75 kHz 1.00×10^{-4}

the number of inner and outer ribs was changed to examine their impact on the mass and stiffness of the membrane. As shown in Table IV, the highest efficiency of 1.4×10^{-4} was obtained for the (3, 12) structure (the first number indicates the inner ribs number and the second one the outer ribs). However, it has also the lowest drum mode frequency of 13.68 kHz. Conversely, the (12, 24) structure gives off the highest drum mode, but lower efficiency. However, the differences between the drum mode frequencies of other structures are not too important, and we have considered the (8, 12) as a good trade-off. Another good point for this structure is the uniform distribution of opening areas, which should be etched in silicon during the fabrication process. Indeed, [35] showed that it is much better for deep reactive ion etching (DRIE) process to have well distributed pattern all over the device surface.

Other structural elements such as the ribs thickness and width, and the central circle radius were chosen in considering the microfabrication limits.

In comparison with [34], the new (8, 12) microstructure theoretically improved the efficiency by more than 60%. According to FEM simulations, structural modes are limited to just two in the considered bandwidth: one at 8.52 kHz (Fig. 5-a) and one at 15.38 kHz (Fig. 5-b). In practice, the first one is less probable to be excited because it is asymmetrical and the driving force is symmetrical. The drum mode at 15.38 kHz is not critical because it occurs in a frequency range for which human ear is not very sensitive.

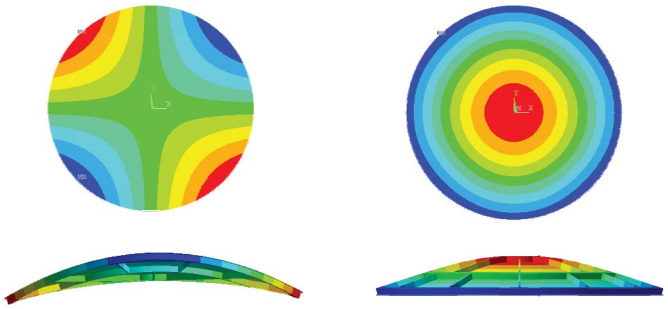

Fig. 5. Two vibration modes of the (8, 12) type reinforced membrane in the range of 300 Hz to 20 kHz.

B. Microcoil and Magnets

The relation between the efficiency, the membrane mass and the electromagnetic parameters can be reformulated as (8) by combining (2) and (7)

$$\eta = \frac{\rho.\pi.r^4}{4c}.\frac{1}{R}.\left(\frac{\sum_{i=1}^{i=n} l_i.B_{ri}}{M_{coil}+M_{membrane}}\right)^2. \quad (8)$$

Here, l_i is the length of the i^{th} coil turn and B_{ri} the radial component of the magnetic flux density observed by the i^{th} turn.

Eq. (8) shows that the coil characteristics intervene in the efficiency via three of its interrelated parameters: its mass, resistance, and length. For this work, the resistance was set at 10 Ω to be compatible with the electronic amplifier circuit, but either the mass or the length of the coil was free to be varied. Since the first two terms of (8) are constant, the third one should be as high as possible to maximize the efficiency. In this way, one solution consists in maximizing the radial component of the magnetic flux density B_{ri}.

To do so, four different configurations of the magnetic part, shown in Fig. 6, were examined. For each case, same total volume and same remnant magnetization of 1.5 T was considered. The radial component of the magnetic flux density in the coil plane was computed using FEM. Variations of the magnetic flux density as a function of the coil displacement were neglected here. This hypothesis is supported by Fig. 7, which shows that for frequencies higher than 2 kHz, the membrane displacement remains in the range of a few microns, that is to say very close to the rest position. Working in lower SPLs, i.e. 70 dB, makes this hypothesis even more realistic in the whole frequency bandwidth.

The radial component of the magnetic flux density as function of distance from the magnets is shown in Fig. 8, for all the four considered configurations. This diagram shows that two magnets face-to-face with axial magnetization is the most interesting configuration because it clearly provides the strongest B_r within a 1.5 mm distance from the magnets. By going beyond this distance, B_r stays close to 0.1 T for all the considered configurations. Furthermore, in order to maximize the flux density observed by the coil, the distance

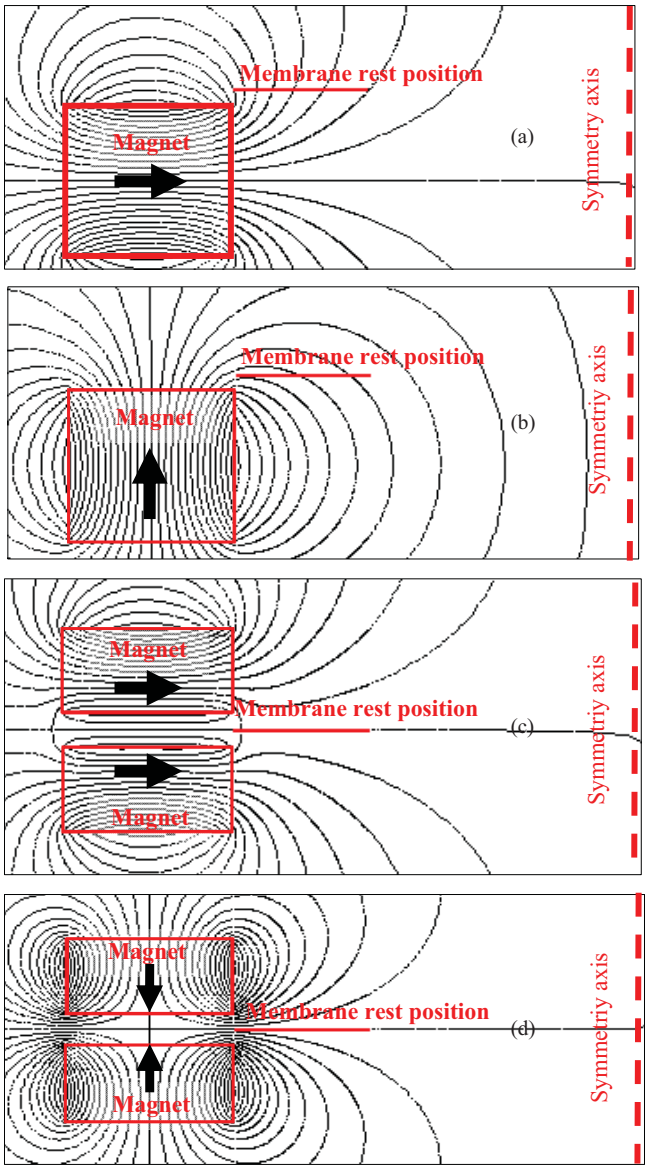

Fig. 6. Distribution of magnetic flux density for (a) one ring magnet with radial magnetization, (b) one ring with axial magnetization, (c) two rings with radial magnetization, and (d) two rings with axial magnetization.

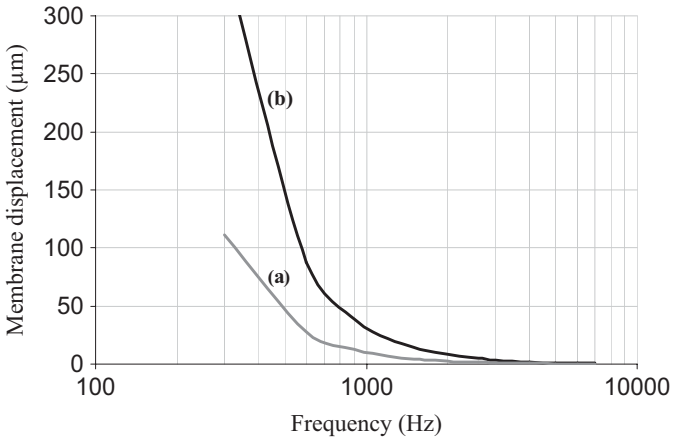

Fig. 7. Membrane displacement as a function of working frequency to produce (a) 70-dB-SPL at 10 cm and (b) 80-dB SPL at 10 cm.

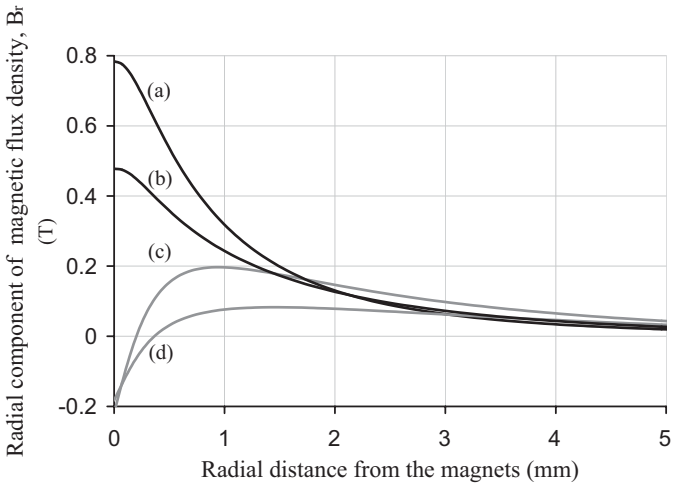

Fig. 8. Radial component of magnetic flux density as a function of distance from the magnet edge for (a) two magnets with axial magnetization, (b) one magnet with axial magnetization, (c) two magnets with radial magnetization, and (d) one magnet with radial magnetization.

between the magnets and coil should be as small as possible: ideally, the coil turns should be concentrated on the edge of the membrane. However, because of technological limits of coil microfabrication, this is not possible in practice.

The copper coil maximum thickness with today's limit of micromolding process is 30 μm. With such thickness, a minimum inter-space of 20 μm between turns was considered in order to obtain a good yield. Finally, the only degree of freedom for the optimization was the coil turn width. Fig. 9 shows that the 35 μm coil width gives the maximum efficiency of 1.28×10^{-4}. Considering the possibility of decreasing the inter-space to 10 μm, with future improvements in the microfabrication process, the efficiency would be increased by 15%.

The efficiency optimization was carried out by successive optimization of the copper microcoil for different values of the membrane mass. Fig. 10 shows the optimum coil mass and the corresponding efficiency as a function of the membrane mass. Each optimized coil corresponds to a realistic configuration which can be microfabricated. According to these results, the membranes with a mass higher than 20 mg need the same 6 mg coil, corresponding to 14 turns of copper with 35×30 μm^2 cross-section and 20 μm inter-space. Beyond 14 turns, the mass of additional turns is not compensated by sufficient gain in force factor. These additional turns are actually farther from the magnets, so they are subjected to lower magnetic flux density. This explains the observed saturation of the coil optimal mass. Conversely, when the membrane mass is below 20 mg, the optimization results show that less coil mass, so less coil turns, yields better efficiency.

IV. Microfabrication

The device microfabrication is based on silicon-on-insulator (SOI) technology. This was chosen because the buried silicon oxide plays a role of stop layer while etching the silicon, and thus provides high thickness precision for the suspension springs and the membrane.

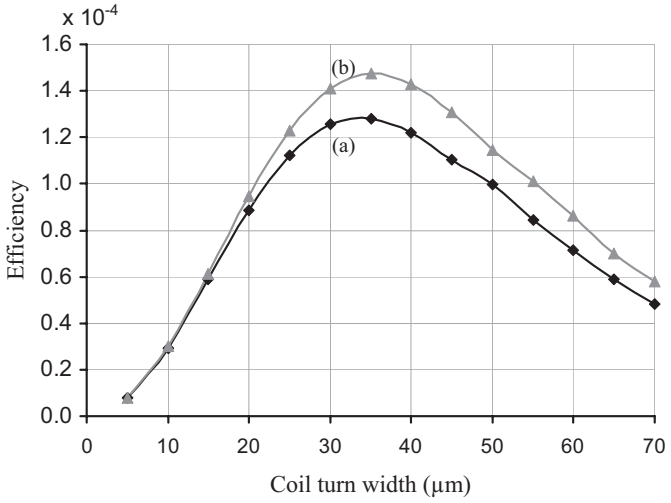

Fig. 9. Efficiency of the microspeaker as a function of the coil turn width for a 30-μm thick coil with 10-Ω resistance and two magnets in 600-μm distance with 1.5 T axial magnetization field (a) 20-μm coil inter-space and (b) 10-μm coil inter-space.

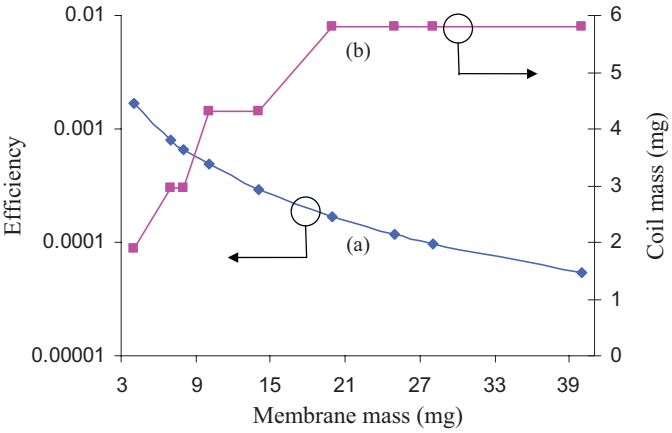

Fig. 10. (a) Optimal efficiency and (b) corresponding mass of the optimized copper coil as function of the membrane mass for the two-ring magnet configuration with axial magnetization.

First, an insulator layer of 200 nm thick silicon oxide is deposited on front side of a SOI wafer by plasma enhanced chemical vapor deposition (PECVD). This layer prevents the short circuits between the conductor tracks. Then, 1 μm thick copper layer is deposited on whole wafer surface by cathodic sputtering. After patterning the copper surface by photolithography resist of Shipley S1818, the wafer is immersed in the copper etch solution for 4 minutes. Once the copper tracks are formed, a second silicon oxide layer is deposited by PECVD to prevent short circuit among coil turns. After S1818 resist patterning, the silicon oxide is anisotropicaly etched using reactive ion etching (RIE) in order to get the two via needed to connect the conductor tracks to the coil inner and outer ends. The suspension beams are then patterned in front side of the SOI using S1828 resist. After etching the silicon oxide by RIE to reach the silicon layer, the 20 μm thick top side silicon layer of the SOI wafer is etched by DRIE. After an oxygen plasma treatment to ameliorate the surface adhesion of the silicon oxide, a 250 nm copper seed layer is sputtered. Then, the copper coil is micromolded. For this purpose, a specific process of spin coating and lithography were developed to obtain a sidewall of 35 μm using Clariant AZ4562 resist. Afterwards, the copper microcoil was electroplated in an electrolyze cell in which the electrolyte was agitated by a magnetic bar at 200 rpm. The most homogenous deposit was realized using -25 mA/cm^2 current density with an anode-cathode distance of 2 cm. After removing the copper seed layer by ion beam etching (IBE), the sample is again spin coated with 35 μm thick AZ4562 in order to protect the coil in final backside etching.

Backside lithography is performed using 10 μm thick Clariant AZ4562 resist. This thickness shows a good masking durability during 300 μm thick silicon DRIE. For this step of the process, the SOI substrate is temporarily bonded in front side to a carrier silicon substrate. To enable good heat transfer during the DRIE process, cooling grease of AlT-CGR7018 is spread out uniformly on the carrier wafer at 70 °C. Then both substrates are aligned and pressed manually to each other. Once the SOI wafer is etched on backside, the carrier wafer is first removed by sliding on sample wafer at 80 °C, and second the coil protection resist is cleaned out in acetone. Finally, the buried silicon oxide layer is removed from the openings in backside by RIE. This step sets the structured membrane free. All these microfabrication steps are depicted in Fig. 11.

V. Characterization

Fig. 12-a shows the contact point between the first interior microcoil turn and the conductor track. As shown on Fig. 12-b, the optical interferometry and mechanical profilometry of the microcoil showed that the electroplated copper is mostly homogenous in thickness: 30 μm$\pm$2 μm. Optical microscopy as well confirmed that no discontinuity does exist in the 60 cm long winding copper coil, confirming the success of the micromolding process.

Electrical characterization of the coil was performed using an impedance analyzer HP 4194A. The current was injected into the terminal connection pads on the sample (Fig. 12-c). Once subtracting the resistance and the inductance imposed by connection wires, the results showed that the coil resistance of 10.3 Ω correlates nicely with theoretical predictions. The coil inductance remains constant, close to 7 μH in the microspeaker bandwidth. The diagram of impedance modulus versus frequency plotted in Fig. 13 shows that from 100 Hz up to 100 kHz the impedance remains stable. This is a good point regarding overall electroacoustic performances of the system.

Fig. 14 illustrates the electromechanical static testing of the membrane out-of-plane displacement as function of input current. These measurements were performed on a test bench using a Keyence LKG5000 laser displacement sensor and a Futek CSG110 force sensor. As can be observed first, very high displacements of 400 μm either upwards or downwards could be reached with no structural failure. Second, the displacement varied linearly from $+400$ μm down to -200 μm, where the line slope changed slightly. This is due to the fact that for these experimental tests, we used a magnet configuration of one ring with axial magnetization. Therefore, the unsymmetrical magnetic field distribution in front and back

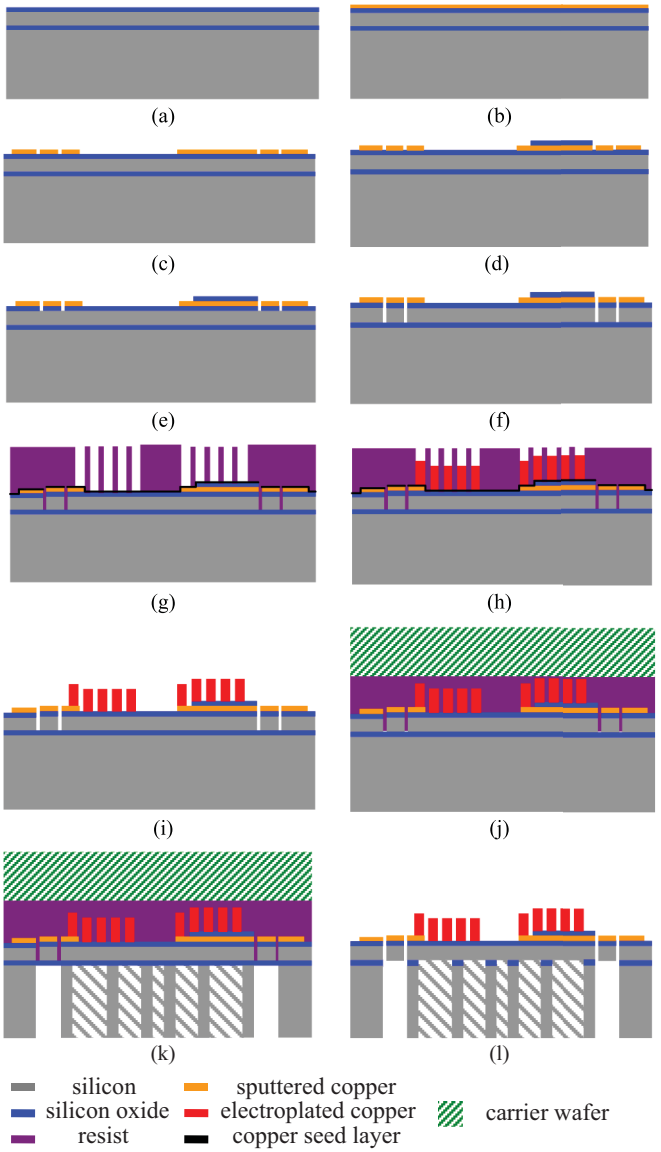

Fig. 11. Microspeaker microfabrication steps. (a) Silicon oxide PECVD. (b) Cathodic sputtering of copper conductor tracks. (c) Copper patterning and etching. (d) Silicon oxide PECVD and patterning. (e) Silicon oxide RIE. (f) Front side silicon DRIE. (g) Cathodic sputtering of copper seed layer and micromolding. (h) Copper electroplating. (i) Mold removing and seed layer etching. (j) Coil protecting with thick resist and temporary bonding. (k) Backside silicon DRIE. (l) Removing the carrier wafer and buried silicon oxide RIE in backside.

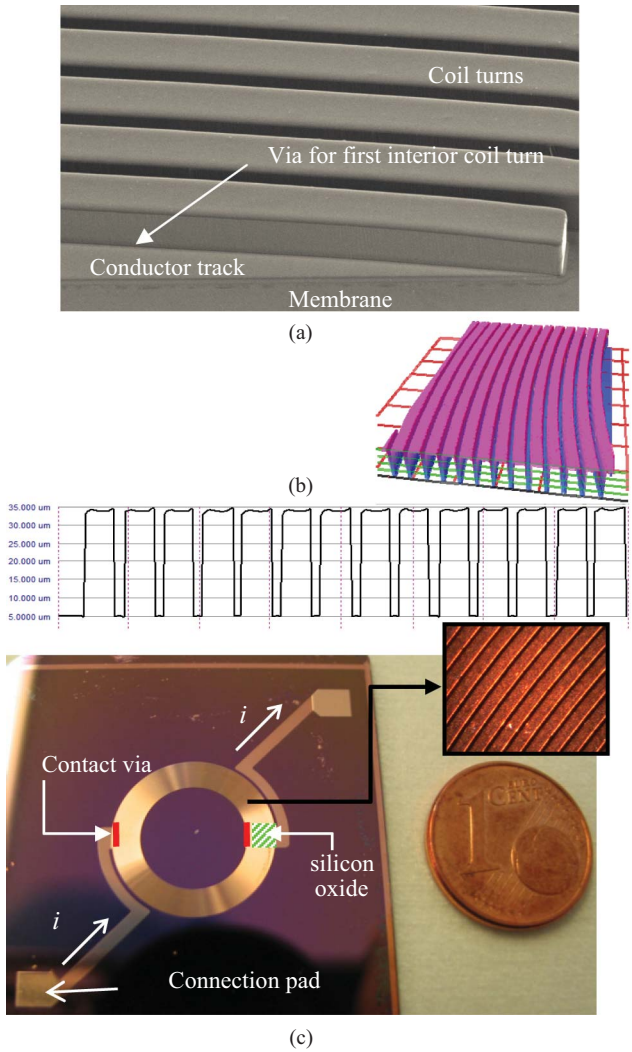

Fig. 12. (a) Scanning electron microscopy picture of the coil turns and the conductor track. (b) Profile of the microcoil measured with optical interferometer. (c) Coil. Inset: copper turns.

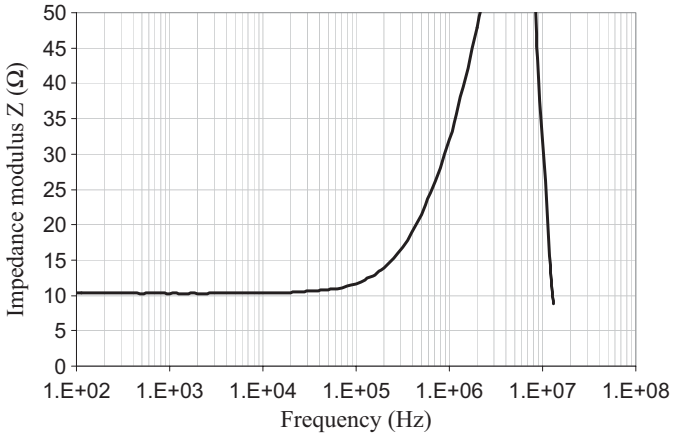

Fig. 13. Impedance modulus measured as a function of frequency for the 30-μm thick copper microcoil.

side of the device resulted in unsymmetrical variations of the force factor.

Finally, acoustic tests were carried out in an anechoic chamber using B&K analyzer and a B&K 4938 microphone set at 10 cm distance from the central axis of the membrane. As depicted in Fig. 15, the first resonance peak in the SPL response takes place at 480 Hz, corresponding to the piston mode of the device. Right after, the SPL stabilizes near 80 dB up to 70 kHz. Thus, acoustics tests showed that the microspeaker is capable to produce high sound intensity at low frequencies. Its cut-off frequency is much higher than the targeted bandwidth. The existence of some peaks and dips in the SPL response could stem from suspensions vibration modes. This point will be investigated in future work. The drum mode was detected near 10 kHz on the measured SPL frequency response, but its presence was not acoustically perceptible.

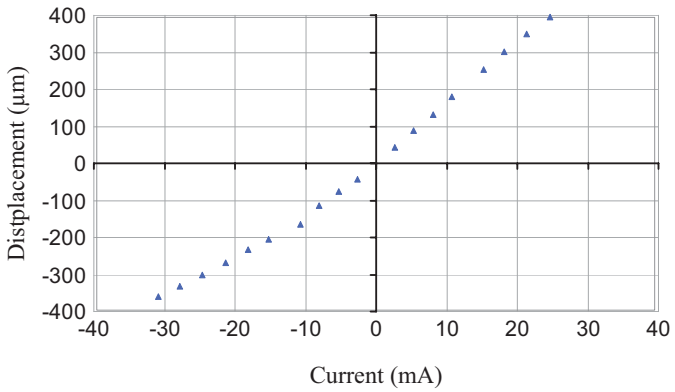

Fig. 14. Membrane static out-of-plane displacement measured as a function of the coil current.

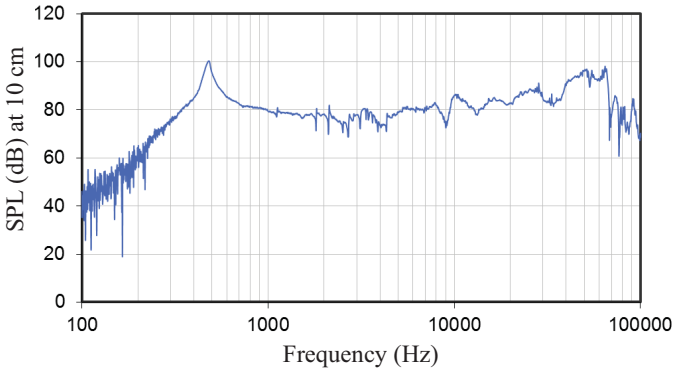

Fig. 15. Sound pressure level (dB) measured at 10-cm distance of the microspeaker, with 0.5 W input power.

One can note that it is difficult to obtain a flat response of the microspeaker in the entire audible frequency range. Moreover, limitations in the low frequencies come from the important volume of air to be displaced by the membrane. Here, the membrane size and its maximum displacement were limited in order to meet integration requirements. This configuration theoretically enables 80 dB SPL at 10 cm starting from 300 Hz. With the same geometrical constraints, less than 70 dB SPL is achievable at 150 Hz. However, the low frequency part of the SPL response of this microspeaker could be improved. Indeed, a flatter response from 300 Hz would be obtained once the piston resonance frequency is shifted below 300 Hz. For this purpose, either a heavier mobile mass or softer suspension should be designed.

Considering the 80 dB SPL response and the injected power of 0.5 W, the microspeaker reached 0.003% efficiency. Although this value remains behind the objective of this work, it is still three times better than typical efficiency of conventional microspeakers used in mobile phones. This value of efficiency was actually obtained by using one magnet ring with axial magnetization, and by deploying a microcoil which was not optimized for this configuration of magnet. Therefore, by replacing one ring magnet with two rings with axial magnetization, as Fig. 8 shows, the flux density is increased by a factor of 1.5. Afterwards, by replacing this flux density in (8) and using the optimized microcoil geometry, the sum of the $B_i.l_i$ is raised by a factor of two. Doubling the force factor multiplies the microspeaker's efficiency by a factor of four. That is to say that experimentally by using two magnet rings and the optimized microcoil, the designed MEMS microspeaker can yield the efficiency of 0.012%. This meets our objective of 0.01% efficiency.

VI. Conclusion

In this paper a novel structure of electrodynamic MEMS microspeaker for mobile electronics applications has been studied. The device optimization in terms of electroacoustic efficiency and sound reproduction quality has been first investigated numerically. Then, experimental results have confirmed the interest of this novel structure and the relevance of the optimization approach.

The originality of the device lies on the use of silicon material for the membrane instead of deformable materials such as parylene or polyimide, as reported in aforementioned works. The properties of polymer materials makes difficult to meet both high fidelity sound reproduction and high efficiency objectives, because the sound radiator should be an extremely light and undeformable surface. This work showed that silicon is one of the most promising materials owing to its high Young's modulus and low mass density. In order to meet both objectives, a particular backside microstructure of the silicon membrane has been studied using FEM simulations. This microstructure shifted most of the membrane vibration modes out of the frequency bandwidth. At the same time, it divided the membrane mass by a factor 5.5.

Apart from the membrane mass, the electroacoustic efficiency depends on the coil mass and the location of the coil turns in the magnetic field created by the magnet. Different magnet configurations were studied. In each case, space distribution of the magnetic flux density was computed using FEM simulations. Then, the planar copper microcoil dimensions were optimized by taking into account the FEM results and the limits of microfabrication. Optimization results showed an electro-acoustic efficiency of 0.0128% with the best magnet configuration. Thus, compared to conventional microspeakers of same size, the proposed MEMS microspeaker has theoretically more than ten times higher efficiency.

The MEMS structure was fabricated using classical silicon micromaching technologies. The main challenges were to micromold the copper coil with thickness as high as 30 μm with good uniformity, and to set free the mobile part of the device with no mechanical failure in the springs.

The electro-mechano-acoustic characterizations showed that the silicon suspension enables membrane out-of-plane displacements of more than 400 μm in amplitude. The sound pressure level measured at 10 cm distance from the microspeaker was near 80 dB, or higher, from 330 Hz to 70 kHz. Compared to conventional microspeakers, this MEMS microspeaker exhibited wider frequency range and higher sound pressure level, especially below 1 kHz. The improvement of the bass rendering (i.e. the acoustic performances in low frequencies) was clearly perceptible. Measurements showed 0.003% electroacoustic efficiency, that is to say three times more than that of conventional microspeakers of similar size and power used in mobile phones.

In this work, a bulk magnet ring was manually aligned with the microcoil. However, no problem related to the coil-magnet misalignment was observed. This can be explained by the fact that the magnet-coil distance was relatively high, larger than 1 mm. In this case, as Fig. 8 shows, misalignments in the range of 200 μm have no important impact on the value of the flux density observed by the coil. This is why the asymmetry of the magnetic force remained negligible. However, either assembling two magnets or decreasing the coil-magnet distance can raise misalignment problems. Nevertheless, such problems can be solved by using high precision automatic pick-and-place tools, as suggested by [13].

Ongoing work focuses on the analysis of total harmonic distortion (THD) and intermodulation distortion (IMD) of the device, in order to deepen the analysis of its electroacoustic quality. The device characteristics will be also analyzed using the two-ring magnet configuration, which should improve both the efficiency and the sound intensity of the MEMS microspeaker.

ACKNOWLEDGMENT

The authors would like to thank the staff of the University Technological Center IEF-MINERVE, Orsay, France, for their help and technical support.

REFERENCES

[1] D. Self, *Class-D Amplifiers*, 5th ed. Waltham, MA: Focal Press, 2009, ch. 13, pp. 366–372.

[2] M. R. Bai, C. Y. Liu, and R. L. Chen, "Optimization of microspeaker diaphragm pattern using combined finite element–lumped parameter models," *IEEE Trans. Magn.*, vol. 44, no. 8, pp. 2049–2057, Aug. 2008.

[3] C. M. Lee, J. H. Kwon, K. S. Kim, J. H. Park, and S. M. Hwang, "Design and analysis of microspeakers to improve sound characteristics in a low frequency range," *IEEE Trans. Magn.*, vol. 46, no. 6, pp. 2048–2051, Jun. 2010.

[4] P. C. P. Chao and I. T. Wang, "Dynamical modeling and experimental validation of a micro-speaker with corrugated diaphragm for mobile phones," *Microsyst. Technol.*, vol. 13, nos. 8–10, pp. 1241–1252, 2007.

[5] K. Lee, Y. Cho, and N. Chang, "High-level power management of audio power amplifiers for portable multimedia applications," in *Proc. IEEE/ACM/IFIP Workshop Embedded Syst. Real Time Multimedia*, Oct. 2006, pp. 41–46.

[6] W. H. Groeneweg, "Analog signal processing for a class D audio amplifier in 65 nm CMOS technology," in *Proc. Solid-State Circuits*, Sep. 2008, pp. 322–325.

[7] C. W. Lin, B. S. Hsieh, and Y. C. Lin, "Enhanced design of filterless class-D audio amplifier," in *Proc. Design, Autom. Test Eur. Conf. Exhibit.*, 2009, pp. 1397–1402.

[8] E. Lefeuvre, I. Shahosseini, J. Moulin, M. Woytasik, E. Martincic, G. Lemarquand, E. Sturtzer, and G. Pillonnet, "Potential of MEMS technologies for manufacturing of high-fidelity microspeakers," in *Proc. Acoust. Conf.*, Apr. 2012, pp. 3093–3198.

[9] S. H. Yi and E. S. Kim, "Piezoelectric microspeaker with compressive nitride diaphragm," in *Proc. IEEE Micro Electro Mech. Syst.*, Jan. 2002, pp. 260–263.

[10] S. H. Yi, M. S. Yoon, and S. C. Ur, "Piezoelectric microspeakers with high compressive ZnO film and floating electrode," *J. Electroceram.*, vol. 23, nos. 2–4, pp. 295–300, 2009.

[11] S. C. Ko, Y. C. Kim, S. S. Lee, S. H. Choi, and S. R. Kim, "Micromachined piezoelectric membrane acoustic device," *Sensors Actuat. A*, vol. 103, nos. 1–2, pp. 130–134, 2003.

[12] M. C. Cheng, W. S. Huang, and S. R. S. Huang, "A silicon microspeaker for hearing instruments," *J. Micromech. Microeng.*, vol. 14, no. 7, pp. 859–866, 2004.

[13] S. S. Je, F. Rivas, R. E. Diaz, J. Kwon, J. Kim, B. Bakkaloglu, S. Kiaei, and J. Chae, "A compact and low-cost MEMS loudspeaker for digital hearing aids," *IEEE Trans. Biomed. Circuits Syst.*, vol. 3, no. 5, pp. 348–358, Oct. 2009.

[14] S. H. Yi and E. S. Kim, "Micromachined piezoelectric microspeaker," *Jpn. J. Appl. Phys.*, vol. 44, no. 6A, pp. 3836–3841, 2005.

[15] H. C. Cho, S. C. Ur, M. S. Yoon, and S. H. Yi, "Dependence of material properties on piezoelectric microspeakers with AlN thin film," in *Proc. IEEE Nano/Micro Eng. Molecular Syst.*, Jan. 2008, pp. 637–640.

[16] S. S. Lee and R. M. White, "Piezoelectric cantilever voltage-to-frequency converter," *Sensors Actuat. A*, vol. 71, nos. 1–2, pp. 153–157, 1998.

[17] P. Rangsten, L. Smith, L. Rosengren, and B. Hok, "Electrostatically excited diaphragm driven as a loudspeaker," *Sensors Actuat. A*, vol. 52, nos. 1–3, pp. 211–215, 1996.

[18] R. C. Roberts, J. Du, A. O. Ong, D. Li, C. A. Zorman, and N. C. Tien, "Electrostatically driven touch-mode poly-SiC microspeaker," in *Proc. IEEE Sensors*, Oct. 2007, pp. 284–287.

[19] Y. C. Chen and Y. T. Cheng, "A low-power milliwatt electromagnetic microspeaker using a PDMS membrane for hearing aids application," in *Proc. IEEE Micro Electro Mech. Syst.*, Jan. 2011, pp. 1213–1216.

[20] J. Rehder, P. Rombach, and O. Hansen, "Balanced membrane micromachined loudspeaker for hearing instrument application," *J. Micromech. Microeng.*, vol. 11, no. 4, pp. 334–338, 2001.

[21] F. L. Ayatollahi and B. Y. Majlis, "Materials design and analysis of low-power MEMS microspeaker using magnetic actuation technology," *Adv. Mater. Res.*, vol. 74, pp. 243–246, Jun. 2009.

[22] R. Rashedin, T. Meydan, and F. Borza, "Electromagnetic micro-actuator array for loudspeaker application," *Sensors Actuat. A*, vol. 129, nos. 1–2, pp. 118–120, 2006.

[23] C. Shearwood, M. A. Harradine, T. S. Birch, and J. C. Stevens, "Applications of polyimide membrane to MEMS technology," *Microelectron. Eng.*, vol. 30, nos. 1–4, pp. 547–550, 1996.

[24] R. Heydt, R. Kornbluh, R. Pelrine, and V. Mason, "Design and performance of an electrostrictive-polymer-film acoustic actuator," *J. Sound Vibrat.*, vol. 215, no. 2, pp. 297–311, 1998.

[25] L. Xiao, Z. Chen, C. Feng, L. Liu, Z.-Q. Bai, Y. Wang, L. Qian, Y. Zhang, Q. Li, K. Jiang, and S. Fan, "Flexible, stretchable, transparent carbon nanotube thin film loudspeakers," *Nano Lett.*, vol. 8, no. 12, pp. 4539–4545, 2008.

[26] H. J. Kim, K. Koo, S. Q. Lee, K. H. Park, and J. Kim, "High performance piezoelectric microspeakers and thin speaker array system," *ETRI J.*, vol. 31, no. 6, pp. 680–687, 2009.

[27] T. D. Rossing, *Handbook of Acoustics*. New York: Springer-Verlag, 2007.

[28] I. Shahosseini, E. Lefeuvre, E. Martincic, M. Woytasik, J. Moulin, S. Megherbi, R. Ravaud, and G. Lemarquand, "Design of the silicon membrane of high fidelity and high efficiency MEMS microspeaker," in *Proc. Design Test Integr. Packag.*, May 2011, pp. 258–262.

[29] A. D. Pierce, *Acoustics*. New York: ASA, 1989.

[30] J. S. Rao, *Dynamics of Plates*. Delhi, India: Narosoa Publishing, 1999.

[31] F. Ke, J. Miao, and Z. Wang, "A wafer-scale encapsulated RF MEMS switch with a stress-reduced corrugated diaphragm," *Sensors Actuat. A*, vol. 151, no. 2, pp. 237–243, 2009.

[32] G. Fragiacomo, T. Ansbæk, T. Pedersen, O. Hansen, and E. V. Thomsen, "Analysis of small deflection touch mode behavior in capacitive pressure sensors," *Sensors Actuat. A*, vol. 161, nos. 1–2, pp. 114–119, 2010.

[33] W. Cui, R. N. Miles, and Q. Su, "A robust miniature silicon microphone diaphragm," *Sensors Transd. J.*, vol. 7, pp. 63–77, Oct. 2009.

[34] I. Shahosseini, E. Lefeuvre, M. Woytasik, J. Moulin, X. Leroux, S. Edmond, E. Dufour-Gergam, A. Bosseboeuf, G. Lemarquand, and V. Lemarquand, "Toward high fidelity high efficiency MEMS microspeakers," in *Proc. IEEE Sensors*, Nov. 2010, pp. 2426–2430.

[35] L. Haobing and F. Chollet, "Layout controlled one-step dry etch and release of MEMS using deep RIE on SOI wafer," *J. Microelectromech. Syst.*, vol. 15, no. 3, pp. 541–547, Jun. 2006.

[36] C. T. Lynch, *Practical Handbook of Materials Science*. Boca Raton, FL: CRC Press, 1990.

[37] M. Madou, *Fundamentals of Microfabrication*. Boca Raton, FL: CRC Press, 1997.

Iman Shahosseini was born in Tehran, Iran, in 1981. He received the B.S. degree in material sciences and engineering from the Isfahan University of Technology, Isfahan, Iran, and the M.S. degree in micro- and nanotechnology from the University of Paris-Sud, Paris, France, in 2003 and 2009, respectively, where he is currently pursuing the Ph.D. degree at the MicroNanoBio and Microsystems Department, Institut d'Electronique Fondamentale. For his Ph.D. research project, he is involved in research on design, microfabrication, and characterization of microelectromechanical systems electrodynamic microspeakers.

He has authored or co-authored more than 15 papers for journals and international conferences.

Elie Lefeuvre received the B.S. degree from the University of Paris-Sud, Paris, France, and the M.S. degree from the Institut National Polytechnique de Toulouse, Toulouse, France, in 1994 and 1996, respectively, both in electrical engineering, and the Ph.D. degree for his research on power electronics converters topologies from the Laval University of Québec, Canada, and the Institut National Polytechnique de Toulouse, in 2001.

He was an Assistant Professor with the Institut National des Sciences Appliquées, Lyon, France. He joined the Laboratoire de Génie Electrique et Ferroélectricité, where he was involved in research on modeling of piezoelectric ceramics, mechanical and thermal energy conversion, and nonlinear switching of ferroelectric materials. He has been with the Institut d'Electronique Fondamentale Laboratory, University of Paris-Sud since 2007, where he is currently a Professor. He has authored or co-authored more than 80 papers in journals and conferences, and two book chapters. He holds four U.S. patents. His current research interests include microelectromechanical systems (MEMS) and nanoelectromechanical systems multiphysics modeling, energy harvesting devices, MEMS sensors and actuators, and microfabrication technologies.

Johan Moulin was born in Marignane, France, in 1971. He received the M.S. and Ph.D. degrees in electrical engineering from École Normale Supérieure de Cachan, Cachan, France, in 1998 and 2001, respectively.

He has been with the University of Paris-Sud, Orsay, France, since 2003, where he is currently an Assistant Professor. He has teaching experience with L'Institut Universitaire de Technologie de Cachan, Cachan, and research experience with the Institut d'Electronique Fondamentale, University of Paris-Sud. He has authored or co-authored 17 articles in refereed journals and 21 conference papers. His current research interests include magnetic material for microelectromechanical systems, and magnetic-based microsensors and actuators.

Emile Martincic was born in Paris, France, in 1969. He received the M.Sc. degree in electrical engineering from the ENSEEIHT of Toulouse, Toulouse, France, and the Ph.D. degree from École Normale Supérieure de Cachan, Cachan, France, in 1998.

He has been with the Institut d'Electronique Fondamentale, University of Paris-Sud, Orsay, France, since 2000, where he is currently an Assistant Professor. He has authored or co-authored numerous papers on microelectromechanical systems (MEMS) sensors and actuators. His current research interests include electromagnetic MEMS.

Marion Woytasik was born in Paris, France, in 1978. She received the M.S. and Ph.D. degrees in applied chemistry engineering from the University of Pierre-et-Marie-Curie, Paris, in 2002 and 2005, respectively.

She was involved in research on microfabrication and characterization of 2-D and 3-D microcoils on flexible substrates. Since then, she is with the MicroNanoBio and Microsystems Department, Institut d'Electronique Fondamentale, University of Paris-Sud, Orsay, France, where she is currently an Assistant Professor. Her current research interests include microfabrication technologies of MEMS and bio-MEMS sensors and actuators.

Guy Lemarquand (SM'09) was born in Paris, France, in 1959. He received the Ph.D. degree in electro-mechanical engineering from Grenoble University, Grenoble, France, in 1984.

He is currently a Professor with the Acoustic Department, Université du Maine, Le Mans, France. His research has encompassed loudspeaker technology and magnetomechanical devices. He has authored or co-authored more than 80 research papers and holds over 30 granted and pending patents. His current research and teaching interests include audio and electromechanical engineering.

Prof. Lemarquand is a Senior Member of the IEEE Magnetics Society and a member of the Audio Engineering Society.